IEEE Open Journal of
Power Electronics

Received 5 October 2022; revised 12 November 2022; accepted 17 November 2022. Date of publication 23 November 2022; date of current version 30 November 2022. The review of this article was arranged by Associate Editor Yingyi Yan.

Digital Object Identifier 10.1109/OJPEL.2022.3223936

Artificial Neural Network Aided Loss Maps for Inductors and Transformers

NAVID RASEKH (Graduate Student Member, IEEE), JUN WANG (Member, IEEE), AND XIBO YUAN (Senior Member, IEEE)

University of Bristol, BS8 1UB Bristol, U.K.

CORRESPONDING AUTHOR: XIBO YUAN (e-mail: xibo.yuan@bristol.ac.uk)

This work was supported in part by the Royal Academy of Engineering.

ABSTRACT The non-linear property of magnetics poses challenges for their loss modelling in power electronics due to lacking full physical models. As a practical approach for their loss estimation, the manufacturers can pre-measure the losses in standalone rigs and distribute the "loss maps" as interpolated look-up tables/curves for the end users. However, with more factors discovered that impact the losses, e.g., DC bias and load conditions, the dimensions of the loss maps cannot be solved by conventional surface/curve fitting methods. This paper addresses this problem by applying the Artificial Neural Network (ANN). For both inductors and transformers, Neural Network-aided loss maps (NNALMs) are designed and evaluated with comparisons against conventional loss maps to reveal the limitations of the latter caused by physically intercoupled input variables. The NNALMs not only show superior accuracy throughout the whole datasets, but also enable the loss maps to expand the dimensions to account for more factors (e.g., load conditions in transformers) and generate multiple outputs (e.g., both the winding loss and core loss). The ANN-aided loss maps can be distributed as digitized datasheets of standardized magnetics, enabling rapid, accurate and user-friendly loss estimations for power electronics engineers.

INDEX TERMS Artificial neural network (ANN), machine learning, loss map, inductor, high-frequency (HF) transformer.

I. INTRODUCTION

Nearly all power electronics applications involve magnetic components for functionality and filtering purposes. As one of the dominant components in size, weight and power losses, magnetics significantly impact the performance of power converters [1], [2], [3], [4]. However, there is no satisfactory first-principle model for core loss in a magnetic component due to the non-linear core loss mechanisms and the intercoupled factors involved, such as the DC bias [5], [6], [7], [8], [9], [10], [11], [12]. In addition, similar to the core loss, the winding loss also partly shares the nonlinearity due to the field interactions with the core and complex geometries, which can hardly be captured by the traditional equation-based methods [13], [14].

While research on non-sinusoidal waves has been extensively studied in recent years, the most widely used core loss models/datasets are still based-on sinusoidal excitations and simplified operating conditions (e.g., ignoring DC bias) [15], [16], [17], [18]. However, the majority of high-frequency magnetics in power converters do not operate with a low-distortion sinusoidal waveform, zero DC bias or room temperature. Therefore, the limited curves and data in a common manufacturer's datasheet cannot factor in all these variables, although some exist models for calculating core losses that factor in temperature based on manufacturer data [19]. Meanwhile, the loss and electromagnetic properties in magnetic materials can vary due to variations in frequency, flux density, DC bias, temperature, and the shape of the excitation waveform, and it is very challenging to measure, store and share all these factors in a manufacturer datasheet [5], [6], [14], [15], [16], [17], [18]. Moreover, geometry-related, component-specific loss mechanisms, such as the gap losses [3], cannot be reflected in the existing datasheets based on materials.

Numerous research efforts have been made to factor in the additional variables contributing to magnetic losses. For

example, [4] proposes to draw the Steinmetz pre-magnetization graphs (SPGs) to reflect the variation of Steinmetz parameters against DC bias levels for core loss. However, this approach does not solve the fitting problem, given that these graphs have no applicable fitting expressions. Moreover, this approach is still limited by the frequency dependency of the original Steinmetz parameters [1] and the dependency on the geometries of individual components (e.g., gap losses [3], ununiform flux distribution [20] and fringing flux effect [21]). To consider the shape of waveforms, an improved generalized Steinmetz equation (iGSE) is proposed in [1], but it cannot solve the non-linear frequency-dependent Steinmetz parameters or the DC bias effect. To consider the gap losses, [3] also proposes to modify the Steinmetz parameters, but it shares the same limitations. In [5] and [8], while the DC bias effect is included, the *dB/dt* and frequency factors are considered independent factors as a simplification to reduce the dimensions and enable fitting, while in fact, these factors are intercoupled with other variables, i.e., H_0 and ΔB.

To address all the above challenges, shifting from material-based to component-based datasheets based on empirical measurements is necessary, especially given the growing popularity of standardized magnetics. Subsequently, for the end users to utilize these measurements, it is crucial to realize standardized loss maps with unified frameworks considering multiple inputs (e.g., *dB/dt*, H_0, ΔB, power factor) and outputs (e.g., core loss, winding loss). For this purpose, machine learning has been proven highly effective in solving non-linear multi-variable classification and regression problems, especially with Neural Networks (NN) [22], [23]. Modelling and designing magnetics in power electronics with the aid of machine learning have been approached in many different ways [15], [16], [17], [18], [24], [25], [26], [27], [28].

For example, the MagNet projects in [15], [16], [17], [18] intend to support data-driven magnetic research using machine learning and neural networks. MagNet stores large quantities of core loss data for many materials measured experimentally under different operating conditions. The input of the MagNet neural network is frequency, voltage/flux-density, duty cycle (single-value), and temperature, and the output is core loss per volume [15], [16], [17]. The voltage and flux density (B) inputs are in the form of time sequence waveforms in three shapes, i.e., sinusoidal, triangular, and symmetric trapezoidal. However, the particular challenge in the case of inductor core loss is caused by the PWM operations in DC/AC converters, which involve varying pre-magnetization (H_0) and varying pulse widths (duty cycle) [5], [6], [7]. As a result, the MagNet NN can only solve the problems in limited cases, e.g., only DC/DC converters with a fixed single duty cycle and H_0 rather than PWM AC/DC converters.

Moreover, with the composite waveform hypothesis (CWH) [5], [6], [7] considered a proven approach to breakdown PWM waveforms and estimating the core loss on a switching cycle basis, the required core loss data only needs to be measured with symmetric 50-50 duty cycle, and there is no need to embed duty cycle as an input variable in the magnetic loss maps. In [18], the input of the NN is a sequence of B (t), temperature, and frequency, and the output is magnetic field intensity, H (t), instead of the core loss per volume. The trained NN obtains the B-H loop and then computes the core loss. The problem with this method, however, is that it might not be suitable to model B-H loops because of its extreme phase sensitivity between the measured and predicted H (t), as the relative core loss error due to the phase discrepancy can be very high and reach 200% and above. The shift error for this work does not relate to the core material and is separate from the phase discrepancy caused by the parasitic inductance of the current sensors, e.g., the current probes. Instead, phase shift here refers to the mismatch between the predicted H (t) and the actual one that can be measured from the experiment.

This paper aims to construct loss maps for magnetic components, given the challenge that multiple inputs and outputs are involved in the loss map, where conventional curves and formulas in the device datasheet are not sufficient to express the non-linear relationships with multiple variables. As a contribution, this work implements and evaluates NN to solve the fitting problem in magnetic loss maps, which has a unified framework and expandability for additional input/output variables. In addition, by comparisons, this study reveals significant errors in the conventional core loss maps due to the oversimplification of intercoupled variables as limited by allowable dimensions. The proposed NN-aided loss map (NNALM) is superior and more user-friendly than the equation-based loss models. Beyond the core loss, this work also extends the loss maps to include winding and total losses as the output and an extended range of interlinked inputs (e.g., temperature, load conditions, etc.) as an engineering solution to provide rapid, accurate and complete loss estimations of individual magnetic components. The proposed NNALM estimation model is for already designed inductors and transformers, which is helpful for magnetic component sellers and power electronics designers rather than for magnetics designers. This paper builds on the authors' previous work on accurate core loss and winding loss measurement and estimation for inductors and high-frequency (HF) transformers [5], [6], [7], [11], [12], [13], [14].

In the following, Section II describes the conventional and component-based loss maps and their limitations in estimating the loss. Sections III and IV present the NN user-friendly loss map for the inductors and HF transformers, respectively, and compare the results with the traditional loss prediction method. This work's practical implementation is also explained in Section V.

II. CORE LOSS MAP APPROACH AND LIMITATIONS

A. CONVENTIONAL LOSS MAP

In empirical core loss models, frequency (f) and flux density swing (ΔB) are essential factors in determining the core loss. The Steinmetz equation (SE) is widely accepted as an

empirically based model for core loss [5] as

$$P_{Core} = k f^{\alpha} \Delta B^{\beta} \tag{1}$$

The Steinmetz parameters, k, α, and β, are obtained by curve fitting. The SE is, however, limited in accuracy, as the coefficients are only accurate within a specific range of frequencies [2]. Additionally, the SE only applies to sinusoidal excitations, meaning it cannot be directly applied to magnetics driven by other excitations, such as PWM. To solve this problem, the improved generalized Steinmetz equation (iGSE) was developed for calculating any arbitrary flux waveform's loss [1] as (T is the period of one cycle)

$$P_{Core} = \frac{1}{T} \int_0^T k_i \left(\left| \frac{dB}{dt} \right| \right)^{\alpha} (\Delta B)^{\beta - \alpha} \, dt \tag{2}$$

With iGSE, SE parameters are converted from sinusoidal to rectangular excitation. iGSE works by breaking down a complex waveform into individual B-H loops. In addition to being widely accepted and proven accurate, the iGSE does not take into account pre-magnetization effects [4].

"Loss map" is an approach proposed in [8] for incorporating DC bias current (I_0) effects. Using experimental B-H loop measurements, a core loss profile can be constructed covering various magnetic components' operating points [9]. As a result, symmetric square-wave excitation of a closed B-H loop is described by three variables, i.e., H_0, ΔB, and flux density change rate $|dB/dt|$, without considering the operating temperature. In repetitive symmetric excitation, $|dB/dt|$ can be converted to f [10]. It is, however, more appropriate to refer to this variable as $|dB/dt|$ rather than the frequency for an instant on the B–H trajectory. Besides, in power electronics, $|dB/dt|$ is proportional to the square-wave voltage amplitude applied to the magnet component [5]. A loss map, or a database of core loss, are therefore functions of these three variables, as follows:

$$P_{Core} = F_1 \left(\left| \frac{dB}{dt} \right|, (\Delta B), H_0 \right) \tag{3}$$

Loss maps generated from finite discrete measurements can be used as look-up tables with interpolations or fitted curves/surfaces [5], [6], [7], [8], [9], [10]. In these references, the assumption is that the core loss is correlated $|dB/dt|$ independently of the other two variables (which is not accurate, as will be explained later) and is expressed as similar to iGSE [4], i.e., $P_{Core} \propto (|dB/dt|^{\alpha})$. To specify the coefficient α, the factor dB/dt can be determined independently by only one data set (fixed ΔB and H_0). Hence, the loss map is simplified by one dimension. Other variables, ΔB and H_0, affect the core loss in a coupled manner. In view of this, a set of datasets covering the possible operating region of interest formed by various ΔB and H_0 are to be assessed as follows, given a fixed (dB/dt) [5].

$$P_{Core} = \left(\left| \frac{dB}{dt} \right| \right)^{\alpha} . F_2 (\Delta B, H_0) \tag{4}$$

To establish the loss maps in this paper, the magnetic structure is excited with a bidirectional half-bridge structure that has been presented in previous studies [5], [6], [7], [11], [12], [13], [14]. Also, a refined discontinuous test procedure as a triple pulse test (TPT) is performed, offered in [5], [6]. Fig. 1 and Table 1 illustrate the utilized experimental test rig and power circuit built in the form of a two-winding method for measuring magnetic component's loss using high-bandwidth voltage and current probes. The measured sensed voltage (v_{Sense}) and excitation current (i_{Exc}) data are then processed in MATLAB as the following expression for the core loss calculation.

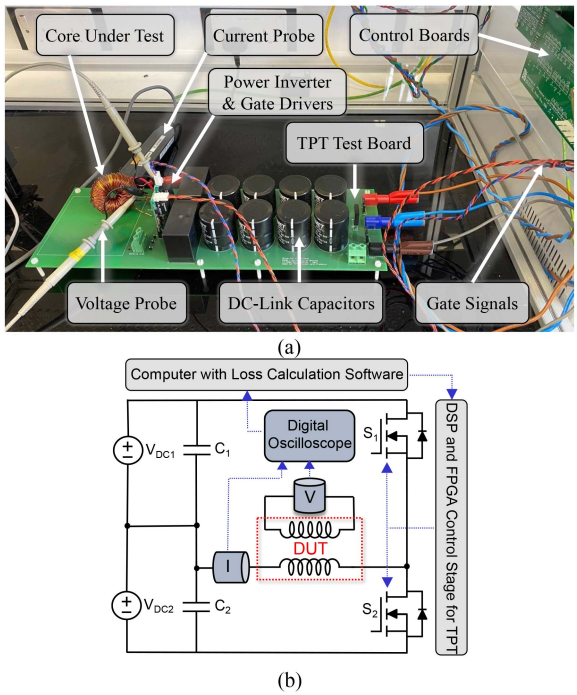

FIGURE 1. (a) The utilized test rig for loss measurements, (b) Simplified schematic of the power stage.

TABLE 1. Components and Instruments in the Test Rig

Power Supplies	Elektro-Automatik TS 8000 T
Voltage Probe	Keysight N2862B (150 MHz)
Differential Probe	Pico TA041 (25MHz)
Current Probe	Keysight N2783B (100 MHz)
Power Device	SiC MOSFET C3M0032120D
Digital Oscilloscope	MSO-X 3054A (500 MHz, 4 GSa/s)
DC-Link Capacitance	2025 µF
Tested Component	92 µH, T184-26, Micrometals©, $N1$:$N2$=24:24

$$P_{Core} = \frac{N_1}{N_2} \frac{1}{T} \int_0^T i_{Exc}(t) \cdot v_{Sense}(t) \, dt \tag{5}$$

N_1 and N_2 are the numbers of the primary and secondary winding turn, respectively. In the later sections, winding and total losses will also be measured using the methods in [13], [14]. In order to reduce phase discrepancy error for measuring the core loss and total loss, the voltage/current probe is aligned using Keysight U1880A deskew tool and calibrated on the oscilloscope with the deskew function. As previously

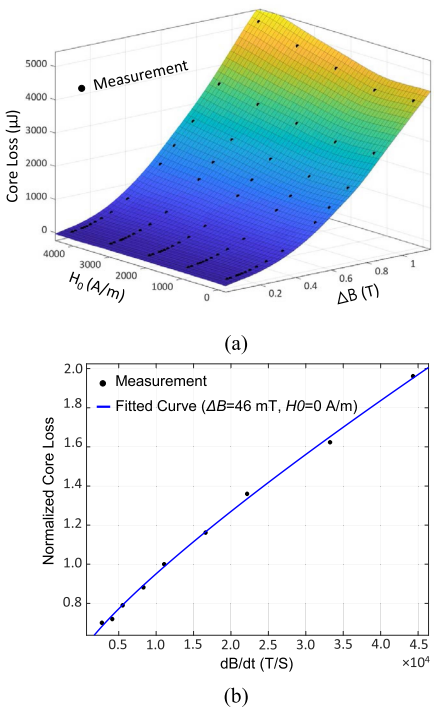

FIGURE 2. **The loss map of the tested component, (a) Core loss versus ΔB, H_0 (dB/dt = 11100 T/s), (b) Core loss versus dB/dt (ΔB = 46 mT and H_0 = 0 A/m).**

evaluated in [11], the deskew method has acceptable accuracy in the broad frequency range by less than a 5% error. Also, the winding loss results are measured by the methods in [13], [14], which are immune to the phase discrepancy error, using the reactive voltage cancellation method.

Two steps are involved in the loss mapping process. Keeping $|dB/dt|$ constant, various ΔB and H_0 operating points are tested as a first step. Fig. 2(a) shows the results as a surface interpolated using Thin-plate splines in MATLAB. For fitting surfaces, the Thin-plate Splines method is one of the most powerful approaches in MATLAB. For the results in Fig. 2(a), the R-square is equal to 1. R-square can take on any value between 0 and 1, with a value closer to 1 indicating that the model accounts for a greater proportion of variance. Also, the sum of squares due to error (SSE) is equal to 4.942×10^{-22}. An SSE value closer to 0 indicates that the model has a smaller random error component and that the fit will be more useful for prediction. These results are shown that the utilized surface fitting method is highly accurate. Besides, the results indicate that it is challenging to fit a generalized expression to ΔB, H_0, and the core loss and problematic to visualize in a datasheet component's loss profile.

The second step is constructing a set of points with constants ΔB and H_0 and varying $|dB/dt|$. Based on this set of data, curve fitting is performed to define parameter α in (4). As seen from Fig. 2(b), the measured data are well fitted to a function with exponential growth. The core loss in Fig. 2(b) is normalized to 11100 T/s (50 V), as the testing voltage and $|dB/dt|$ for Fig. 2(a) are $\pm$50 V and 11100 T/s, respectively. In summary, the core loss can be obtained from a loss map in two steps: 1) find the energy using ΔB and H_0 in Fig. 2(a), and 2) scale the energy to the testing voltage using $|dB/dt|$ in Fig. 2(b).

B. COMPONENT-BASED (RATHER THAN MATERIAL-BASED) LOSS MAP

A precise and convenient loss map can be attained if the loss data is captured from the same core material, shape, and winding arrangement of the aim magnetic device (component-based), as explained previously in [5], [6], [14], in contrast to conventional material-based loss maps. This is because, with the same core/winding material, each component built can have different characteristics, e.g., the core gap loss cannot be captured by the material-based dataset. In addition, in power electronics, it is common to use electrical and time-domain variables as opposed to magnetic variables in the loss map. The translation between these variables complicates calculating core losses and loss mapping. Additionally, due to manufacturing tolerances, magnetic components have batch-to-batch variations on their geometries/characteristics, which can subsequently lead to slight loss variations.

In order to simplify core loss estimation and to facilitate a straightforward loss map procedure, a method has been developed in [5] that relies solely on time-domain and electrical variables, replacing the conventional magnetic variables. Using the user-friendly loss map, one operating cycle of a magnetic component can be characterized by three variables: primary voltage (V_{Pri} as dB/dt), volt-second product (V_{Pri} . T as ΔB), and DC bias current (I_0 as H_0). This allows the loss map to be expressed as (6)

$$P_{Core} = F_3\,(V_{Pri},\ V_{Pri}\,.\,T,\ I_0) \tag{6}$$

Compared to the magnetic-domain loss map shown in Fig. 2, this loss map will not only simplify core loss calculation, but also simplify the loss mapping process that only needs to include the 50% duty cycle with the CWH approach [7]. Using the user-friendly loss map with an aimed operating point, the TPT's electrical and time-domain parameters (pulse width and height) can be derived directly without having to translate from magnetic to electrical domains. This idea is to have a component-based loss map - the tested component should be identical (or at least representative regarding physical structure) to the component to be predicted. This loss map can be a practical idea of what new loss datasheets will look like for the pre-characterized inductors/HF-transformers, analogous to the commercial switching devices' loss data [5], [6], [14].

Similar to the core loss, the winding loss characteristic is subject to the large-signal level, as investigated in [13] and [14]. Also, the measured winding AC resistance is found to be correlated with the load level/feature in HF transformers. Hence, on the condition that the experimental measurement carries out on the specific magnetic component design, and to simplify/improve the loss extraction process, the measured

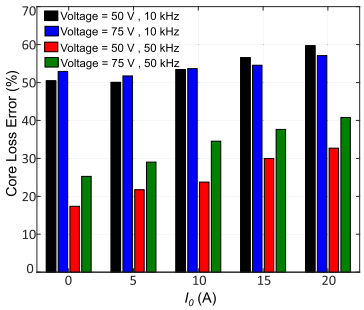

FIGURE 3. Error of core loss calculated from datasheet against measurement results.

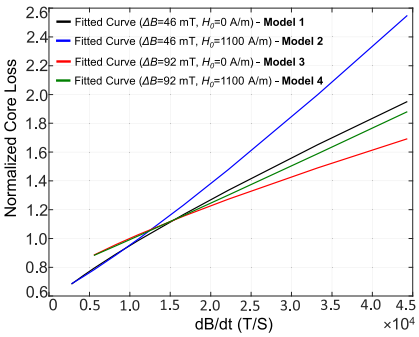

FIGURE 4. "|*dB/dt*|" scaling models - core loss versus *dB/dt* and various fixed conditions of ΔB and H_0.

winding loss, together with the core loss (total loss), can be distributed in the form of a user-friendly loss map [6], [14]. As a result, these three variables also describe the winding loss. DC winding loss can be expressed with I_0. Another two variables as V_{Pri} and V_{Pri} . T, demonstrate individual square excitation and the waveform of current flowing in a magnetic component, which indicates the ac loss of winding.

C. LIMITATIONS

Using the loss map approach developed in previous studies in practice is not straightforward. It is impossible to provide all potential scenarios designers may have to deal with in classical datasheets for magnetic materials. To begin with, a conventional loss map is usually offered and used as a three-dimensional look-up table presented in a datasheet [8], [9], [10]. Although it will be more feasible for manufacturers to print the energy loss suggested in [5] against electrical parameters on datasheets, neither the user nor the loss map can accurately interpret or cover the full range of possible data points.

Furthermore, the loss map has limitations regarding the number of variables and how they should be displayed. A datasheet cannot accurately predict the behaviour of magnetic materials under sophisticated operating conditions [18]. Aside from the three variables in the loss map, some other parameters, such as the temperature, also affect the loss value. Besides, when it comes to HF transformers or coupled inductors, the load's type/value, as well as the power factor, contribute to the core and winding losses [12], [14]. Thus, the parameters will be increased from 3 to 6 as voltage, frequency, DC bias current, temperature, load impedance, and power factor. This detailed loss map cannot be displayed in a graph or look-up table like Fig. 2 in datasheets, and the loss cannot be easily read and obtained by curve/surface fitting.

To show the difference between the most conventional model and the TPT measurement, the core loss is calculated based on the magnetic core's datasheet and compared with measurement results in Fig. 3. The conventional datasheet, such as the one used in [29] provides a core loss formula based on the sinusoidal excitation with two input variables: peak flux density and frequency. Also, the peak flux density should be calculated with a separate equation based on the excitation voltage, frequency, and magnetic core properties, i.e., winding number of turns and core cross-sectional area. This method ignores the DC bias effect and the difference between sinusoidal and rectangular waveforms. The result reveals that the datasheet core loss differs significantly from the measured ones. Increasing the DC bias current increases the error since the conventional datasheets cannot account for the DC bias effect. Therefore, as also stated in [4], [5], traditional loss datasheets and methods based on sinusoidal excitation are unreliable tools for predicting square voltage excitations with DC biases.

As another important limitation in conventional-fitting-based loss map, Fig. 4 shows that the loss scaling over $|dB/dt|$ is correlated to the other two variables, which means the three variables (H_0, ΔB, and $|dB/dt|$) are physically intercoupled with each other. This demonstrates that the conventional loss map approach ([4], [5]) made an oversimplification to consider the $|dB/dt|$ as an independent variable, as in (4) and (6). The four models shown in Fig. 4 are later applied in Section III as examples.

This work aims to overcome these limitations by implementing neural networks in a user-friendly digital loss map. NNALM can resolve the problem related to the different and multiple input and output parameters. NNALM is, therefore, superior to conventional surface/curve fitting that is prone to error and difficult to display in datasheets. NN files, which are only a few kilobytes in size, only need to be trained and provided by the manufacturers to the user for each magnetic component in a user-friendly loss map format. The NNALM for inductors and HF transformers will be discussed in the next two sections, along with the error regarding conventional loss maps compared to the NNALM.

III. NN AIDED INDUCTOR LOSS MAP

This Section introduces the neural network structure used in the user-friendly loss map for inductors. A comparison is then made between the NNALM and the conventional loss maps for the core loss of the inductors.

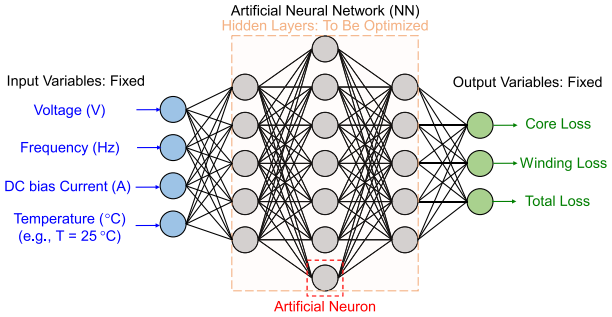

FIGURE 5. An example of NNALM structure for the inductors with four inputs, three outputs, and three hidden layers.

A. NNALM STRUCTURE

The neural network is the most commonly used and straightforward method for solving multi-variable non-linear regression problems [15], [16], [17], [18]. Magnetic components can be designed/modelled more effortlessly with NNs, which have proven effective in solving problems where precise physical understanding does not exist [24], [25], [26], [27], [28]. This part uses an NNALM to develop and digitalize a user-friendly loss map model for inductors. An example of a 5-layer NNALM is shown in Fig. 5. Specifically, this network has one input layer, one output layer, and three hidden layers. As a result of using a user-friendly loss map, the input layer has four input variables: the inductor primary voltage, excitation frequency, DC bias current, and temperature. Three parameters are included in the output layer: core loss, winding loss, and total loss, which can be in different units like Joule or Watt. The total loss can be obtained simply by summating the core and winding losses or using the direct total loss approach using the two-winding method and primary voltage [14]. NNALM with a total loss is an accelerated option for the power electronics designers to know the entire loss of the magnetic components when the separated loss is not of interest.

The hidden layers contain multiple neurons, and the number of layers and neurons in the hidden part should be optimized. It has to be noted that the choice of the ANN structure is not unique, and many different structures may give good performances. Also, regarding the number of layers and neurons, there is no general principle to determine their exact numbers [24]. A trade-off between network size and performance needs to be considered when determining the number of neurons in each hidden layer [15], [16], [17], [18], [22], [23], [24], [25], [26], [27], [28]. A small network may have limited learning capability and cannot provide good predictions, while a large network is more prone to overfitting. ANN designers often use trial and error to find the best performance for their system, which has also been done in this work [24]. Using the trained NN, the user can attain the magnetic component losses based on input parameters. For an accurate NN to be trained, it is essential to have a considerable amount of reliable data, particularly data collected under different conditions. Initially, a large dataset of measurements is collected, and then core and winding losses are calculated, as the data acquisition part described in Section II-A. The NN is trained using these data, and its structure and parameters are saved when the training is complete. The NN can finally be used directly to predict losses for user-defined inputs.

This work uses the built-in MATLAB neural network Toolbox as a NN engine. The NN is designed as a two-layer feedforward network with 15 sigmoid hidden neurons and linear output neurons, which is suitable for regression tasks [25], [30]. Based on the results in the following, a 15-neuron structure per hidden layer is a good balance between performance and computational cost in this work. It is worth mentioning that the use of shallow neural networks may not pose a challenge regarding computational cost. Consequently, overfitting could serve as a better criterion for the network scale of the shallow NN with only one hidden layer. The Toolbox training process determines the weights and biases of the NN automatically. Three subsets are randomly selected from the entire dataset: a training set (70%), a validation set (20%), and a test set (10%). A Levenberg-Marquardt backpropagation algorithm with mean square error as a metric is employed for the training algorithm. To determine if overfitting is occurring, the error metrics of the training and validation subsets are compared in the Toolbox automatically.

For the inductor case, the dataset includes 75 core losses, 75 winding losses, and 75 total losses; in different excitation voltages, frequencies and DC bias currents. Due to the short testing transition (e.g., $<100\ \mu$s) of each run, the temperature in the TPT does not cause a temperature rise in the testing. Therefore, all experiments in this paper are conducted at room temperature (e.g., T = 25 °C). Although the temperature is not evaluated as a variable in this work, the ANN-aided loss map can include the temperature effects as one additional input variable, given it can change the loss significantly [15], [16], [17], [18]. Though, adding the temperature to the conventional loss maps as one additional dimension is difficult due to the limitation of fitting – in this sense, only ANN-aided loss maps can facilitate this one extra variable considering the possibility that it could be coupled with other variables due to cores' nonlinearity. As a result, the NNALM can include the temperature factor if needed, as indicated in Fig. 5.

Fig. 6 depicts the predicted NNALM results and measured loss for the inductor case. The results demonstrate a solid alignment of the data points around the reference target (Predicted = Measured, $Y_{Axis} = X_{Axis}$). Although the test set is not large and the NNALM results can be improved by enhancing the database, the predicted value has demonstrated acceptable and consistent accuracy. Also, Fig. 7 shows the histogram, a graphical representation of data points and the relative error between the predicted NN and reference values.

Fig. 8(a)–(c) compares the NN predicted and measured losses of the inductor core, winding, and total, in different ΔB values. In Fig. 8(a)–(c), the voltage is selected as 25 V, 50 V, and 75 V, and the frequency is selected as 10 kHz, 15 kHz, 20 kHz, 50 kHz, and 100 kHz. DC bias current in these

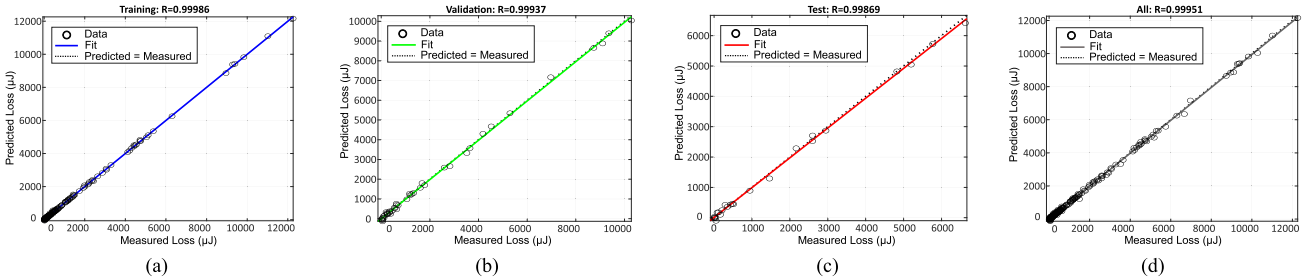

FIGURE 6. NN loss prediction results against the inductor's measured values for (a) Training set, (b) Validation set, (c) Test set, and (d) All the data sets.

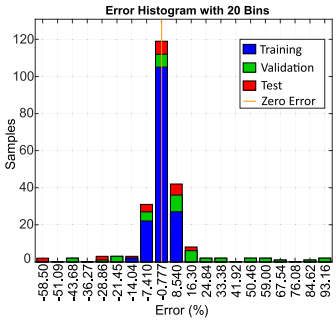

FIGURE 7. The error histogram of the three different data sets of the inductor.

circumstances is 0 A, 5 A, 10 A, 15 A, and 20 A; therefore, each loss in Fig. 8 has 75 data points. As the ΔB is proportional to the inductor voltage and frequency, the data points are scattered, similar to those shown in Fig. 8(a)–(c). Results from the neural network demonstrate that it can achieve comparable results to TPT measurements and effectively trace the results. For quantitative analysis of loss prediction accuracy, the relative error between measured losses and predicted losses is calculated as follows and depicted in Fig. 8(d) for each sample:

$$Loss\ Error\ (\%) = \left(\frac{P_{\text{Measured}} - P_{\text{Predicted}}}{P_{\text{Measured}}}\right) \times 100 \quad (7)$$

According to (7), the calculated error can be negative when NNALM predicts a loss that is more than the measured value. Thus, the average error should be calculated using the absolute value of the relative errors. Despite a few data points with errors exceeding 50%, for the core loss, winding loss, and total loss sets, the average relative error (*ARE*) is 8.32%, 10.14%, and 6.61%, respectively. Hence, the average relative error is within 10% in all three cases.

B. CORE LOSS MAP COMPARISON

In this part, the results of the inductor NNALM and conventional loss map are compared in various conditions. In the first case, the excitation frequency and DC bias current are fixed to 35 kHz and 0 A, respectively, and the voltage/flux density varies. In this Section, neither the NNALM nor the conventional loss map (surface fitting method) does not include the target test data, so the results should be entirely predicted. Based on the conventional loss map proposed in Fig. 2 and the NNALM results, Fig. 9 illustrates the core loss comparison for the inductor when the curve fitted of core loss versus *dB/dt* fixed at $\Delta B = 46$ mT and H_0=0 A/m (Model 1).

According to Fig. 9(b), the calculated error between the reference measured value and the NNALM is much lesser than the surface fitting method, especially in the lower ΔB. Although the data in lower ΔBs are more in number in Fig. 2(a) compared to the higher ΔBs in the surface fitting, the average error value for the NNALM is around 8.31%; however, the conventional loss map is about 53.70%. Since the core loss is much smaller in the lower ΔBs, surface fitting cannot provide an accurate prediction in this area of the loss map, and only a slight discrepancy can make a considerable error.

Applying the different four models shown in Fig. 4 to factor in *dB/dt*, Fig. 10 displays the core loss results and the calculated error against the reference measured value for each case. As described previously in Section II-C and depicted here, the core loss is closely related to all three parameters in the conventional loss map, and the results are significantly affected by the different core loss scaling models versus *dB/dt* curves. In comparison to NNALM, this is one of the main disadvantages of the surface fitting. For better comparisons, it is helpful to note that NNALM results are close to measurement results in Fig. 10, as demonstrated before in Fig. 9(a).

In the next case, the excitation frequency and DC bias current increase to 75 kHz and 2 A, respectively, and the voltage/flux density varies. Fig. 11 shows the core loss results, the error difference between the two methods and the reference value.

Similar to Fig. 9, the error between the reference measured value and the NNALM is lower than the surface fitting method. The average error value for the NNALM is around 9.45%, and the conventional loss map is about 50.86%. Fig. 12 displays the core loss of the measurement and the conventional loss map methods when using different fitted curves for the core loss versus *dB/dt* curves; and the calculated error between the reference measurement value and various surface fitting results. The average error value for the various curves in Fig. 12(b), from black to green, is around 50.8%, 48.4%,

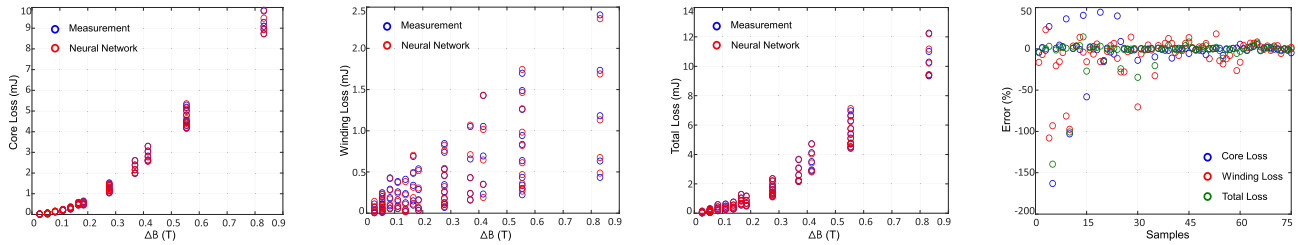

FIGURE 8. The NN predicted and measured losses of the inductor for (a) Core losses, (b) Winding losses, (c) Total losses, and (d) the calculated relative errors.

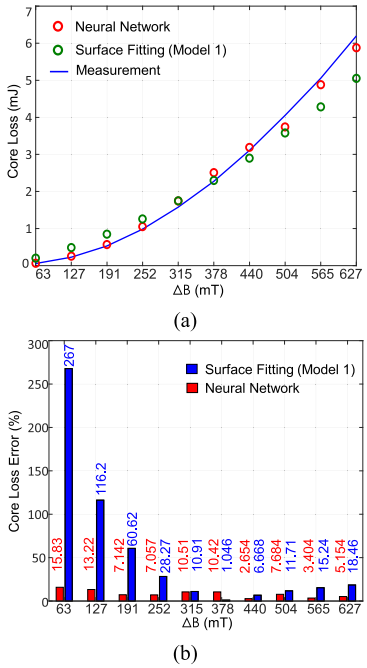

FIGURE 9. (a) The core loss results from measurement, NN, and surface fitting, (b) the calculated error between the measured results and the NN and surface fitting methods.

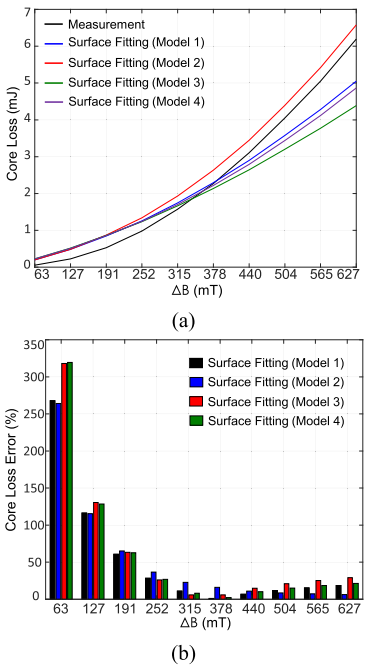

FIGURE 10. (a) The core loss of the measurement and the conventional loss map methods when using different fitted curves for the core loss versus *dB/dt* curves, (b) the calculated error between the reference measurement value and various surface fitting results.

60.8%, and 58.2%, which confirms that different curves resulted in varying accuracy levels in conventional loss maps.

In the following case, the excitation voltage and DC bias current are fixed to 100 V and 0 A, respectively, and the excitation frequency/flux density varies. A comparison of different methods and the reference value is shown in Fig. 13. The error between the reference measured value and the NNALM is lower than the surface fitting method, similar to the results in Figs. 9 and 11. The average error value for the NNALM is around 9.88%, and the conventional loss map is about 65.07%. Similarly to the previous results, error increases when ΔB, as well as the core loss, is decreased in the conventional loss map method.

Fig. 14 indicates the core loss along with the conventional loss map when using different fitted curves for the core loss versus *dB/dt* curves and the calculated error between the reference measurement value and various surface fitting results. The average error value for the various curves in Fig. 14(b), from black to green, is around 65.0%, 78.9%, 59.1%, and 61.8%, clarifying that various fitted curves cause different loss estimations.

C. SUMMARY

As the results show, surface fitting is incapable of predicting the loss with precision in different situations, especially where the core loss is small and can be significantly changed by a minor wrong prediction. In addition, the obtained loss is remarkably changed with the conventional loss map method by selecting different fixed sets of ΔB and H_0 for the fitted curve, similar to Fig. 4. This difficulty has therefore been addressed

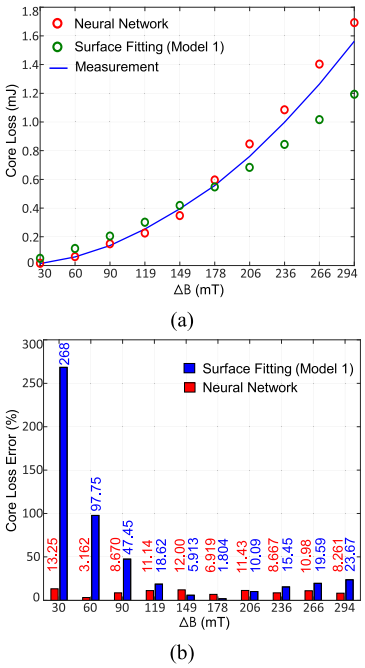

FIGURE 11. (a) The core loss results from measurement, NN, and surface fitting, (b) the calculated error between the measured results and the NN and surface fitting methods.

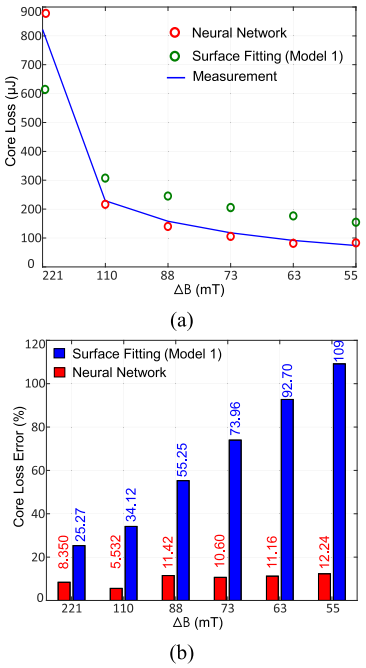

FIGURE 13. (a) The core loss results from measurement, NN, and surface fitting, (b) the calculated error between the measured results and the NN and surface fitting methods.

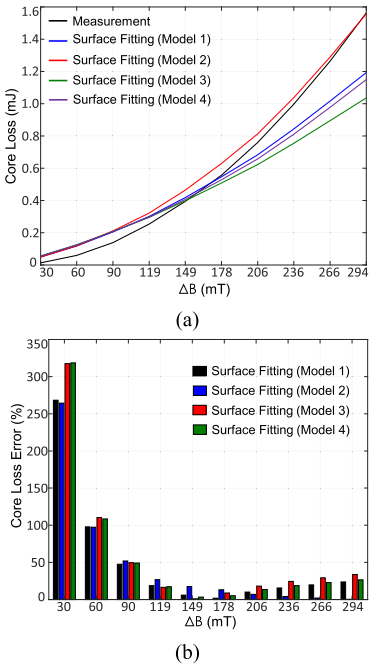

FIGURE 12. (a) The core loss of the measurement and the conventional loss map methods when using different fitted curves for the core loss versus *dB/dt* curves, (b) the calculated error between the reference measurement value and various surface fitting results.

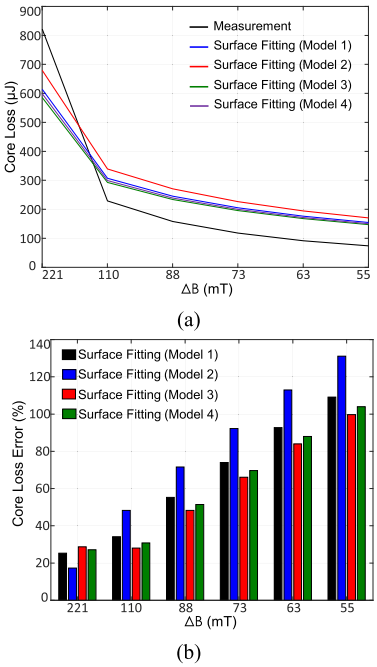

FIGURE 14. (a) The core loss of the measurement and the conventional loss map methods when using different fitted curves for the core loss versus *dB/dt* curves, (b) the calculated error between the reference measurement value and various surface fitting results.

using the NNALM. In every tested case, NNALM could trace the measured loss accurately and predict it, resulting in an average error of less than 10%. By enhancing the database, both the conventional loss map and the NNALM methods can be improved, but the curve fitting problem for the loss map cannot be solved since the core loss parameters are interconnected. Furthermore, even other parameters like temperature can change these fitted curves. Therefore, NNALM can be more practical for estimating the loss, which is easier to be used by the user with the user-friendly loss map inputs. In this way, power electronics designers will no longer have to spend hours extracting and extrapolating parameters from datasheets prone to accessibility or clarity issues.

IV. NN AIDED HF TRANSFORMER LOSS MAP

NNALM for HF transformers is introduced in this Section, where a greater number of input parameters should be included to ensure accuracy, which is beyond the capabilities of conventional models. Besides the four input variables in the loss map, some other parameters also affect the loss value. In addition to the temperature, the load condition can affect HF transformers' core and winding losses [12], [14]. Different load conditions change the primary and secondary currents' amplitude and power factor, resulting in changes in the loss. Hence, it is crucial to include more input parameters in the NNALM than previously proposed ones.

Both the magnitude and phase of the load impedance can affect the loss. There are different ways in which load impedance can be incorporated into the NNALM, depending on the loss map creators or applications of the HF transformer. The impedance magnitude can be expressed with the ohm unit, and the impedance phase can be characterized by the load power factor, as used in this work for input variables. Depending on the application, for example, if the load is in inductive form, the inductance in H or inductive reactance in ohm can be included instead of the power factor in the NNALM for simplification, besides the impedance resistive magnitude. This allows the user to obtain accurate loss values by adding load information, such as magnitude in ohm, alongside the power factor to the NNALM.

As an example, a 5-layer HF transformer NNALM is shown in Fig. 15, with six inputs, three outputs, and three hidden layers. Similar to the inductor NNALM, The NN is designed as a two-layer feedforward network with 15 sigmoid hidden neurons and linear output neurons. A total of three subsets of the dataset are chosen randomly: a training set (70%), a validation set (20%), and a test set (10%). The training algorithm employs Levenberg-Marquardt backpropagation with mean square error as a metric. For the HF transformer case, the dataset includes 375 core losses, 375 winding losses, and 375 total losses; in different excitation voltages, frequencies, DC bias currents, and load conditions. Due to the TPT, all dataset temperatures are at T = 25 °C and have the same environment temperature, which means the thermal effects have not been included in this NNALM. Moreover, if the no-load condition

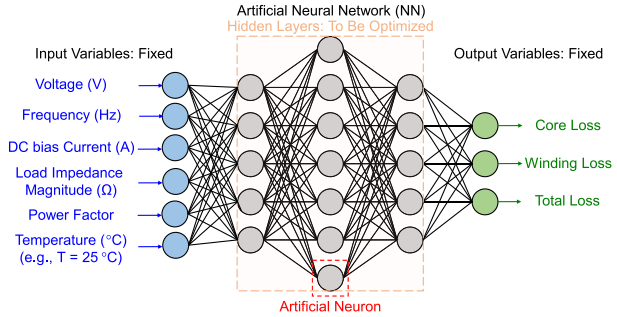

FIGURE 15. An example of NNALM structure for the HF transformers with six inputs, three outputs, and three hidden layers.

TABLE 2. Prediction Results for Different Types of Loss

Magnetic Component Loss	*ARE*	*RMS*	*RSE*
Inductor Core Loss	8.32 %	9.12 %	1.0062
Inductor Winding Loss	10.14 %	10.86 %	0.9895
Inductor Total Loss	6.61 %	7.03 %	1.0045
Transformer Core Loss	7.51 %	8.47 %	1.0013
Transformer Winding Loss	7.89 %	8.92 %	0.9947
Transformer Total Loss	3.48 %	4.50 %	1.0008

for the input values is selected, the transformers NNALM can also be used for the inductor cases as well.

Fig. 16 depicts the predicted NNALM results and measured loss for the transformer case. The results demonstrate a satisfactory alignment of the data points around the reference target (Predicted = Measured, $Y_{Axis} = X_{Axis}$). Additionally, Fig. 17 shows the graphical representation of data points and the relative error between the predicted NN and reference values.

Fig. 18(a)–(c) compares the NN predicted and measured losses of the HF transformer core, winding, and total, in different excitation conditions. NNALM has demonstrated that it can achieve results comparable to TPT measurements and trace them effectively. Despite a few data points with errors exceeding 50%, for the core loss, winding loss, and total loss sets, the *ARE* is calculated from (7) and shown in Fig. 18(d) as 7.51%, 7.89%, and 3.48%, respectively. Thus, the average relative error is less than 8% in all three cases.

Table 2 summarizes different evaluations for the NNALM output of the inductor and HF transformer used. The R-Squared-Error (*RSE*) closer to one implies a higher prediction accuracy from the NNALM [15], which is defined as follows:

$$RSE = \frac{\sum \left(P_{\text{Predicted}} - \bar{P}_{\text{Measured (Average)}}\right)^2}{\sum \left(P_{\text{Measured}} - \bar{P}_{\text{Measured (Average)}}\right)^2} \tag{8}$$

The NNALM is more accurate in predicting transformer losses due to a four-fold increase in the dataset from the different input conditions, compared to the inductor case by roughly 30%. For both the transformer and inductor cases, the ANN structure used in this paper has less than 10% average error for each of the three outputs: core loss, winding loss, and total loss. To illustrate how the error changes across various

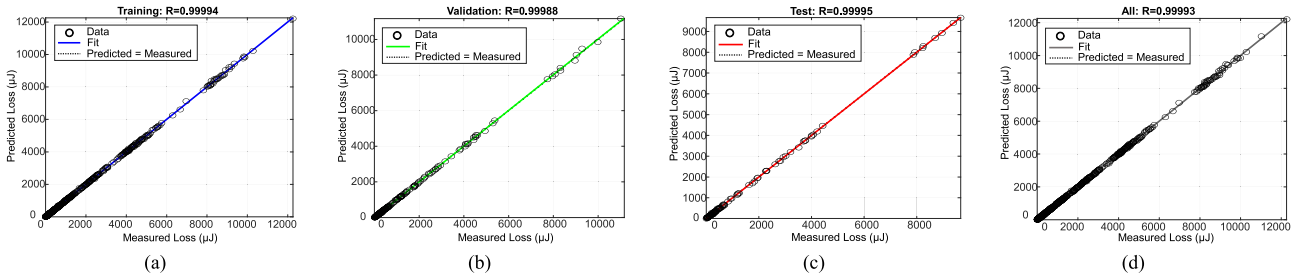

FIGURE 16. NN loss prediction results against the HF transformer's measured values for (a) Training set, (b) Validation set, (c) Test set, and (d) All the data sets.

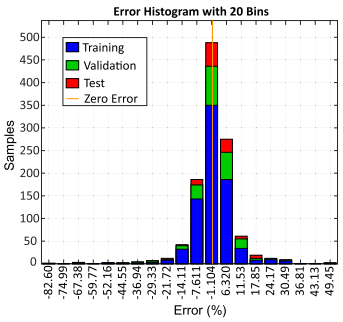

FIGURE 17. The error histogram of the three different data sets of the transformer.

ANN structures, for instance, with decreasing the number of neurons to 10 from 15, the average error for the inductor case is less than 20%, and for the transformer case, it is less than 18%. For another example, by fixing the number of neurons to 15 and adding one more hidden layer, the average error for the inductor case is less than 17%, and for the transformer case, it is less than 13%. Therefore, as explained, there is no general principle to determine the exact numbers of layers and neurons, and each structure can change nonlinearly.

Fig. 19 presents the results of the HF transformer NNALM and conventional loss map in various load impedance magnitudes. Dc bias current, excitation voltage, frequency, and power factor are set to 0 A, 50 V, 50 kHz, and one, respectively. The *dB/dt* fitted curve does not need to be used here as the voltage is set to 50 V.

Similar to the results for the inductor case, the error between the reference measured value and the NNALM is lower than the surface fitting method. NNALM's average error value is around 7.77%, while the conventional loss map method is about 44.11%. In line with the previous results, the error increases slightly when ΔB, as well as the core loss, is decreased in heavier loads [12] for the conventional loss map method.

In some cases, manufacturers may not be feasible to build a loss measurement platform and collect enough reliable data for model training, especially if multiple factors are included, similar to the HF transformer cases. To overcome the data limitations, transfer learning techniques can be applied [16]. Machine learning techniques, such as transfer learning, use the knowledge gained from solving one problem to solve a related one. In transfer learning, the principal goal is to reduce the amount of new data required. To begin with, a generic model that captures the common characteristics and patterns of magnetic component losses should be created (like the no-load condition or inductor case) and then used to develop loss models for other specifications, such as other load values or power factors, through transfer learning. As a result, many different load conditions do not need to be measured for the HF transformer database, facilitating the data acquisition process.

To sum up, the NNALM is a valuable tool to assist the power electronics designer in estimating the magnetic component losses, particularly for the higher input parameters condition such as HF transformers or coupled inductors, which is challenging or impossible with other methods.

V. PRACTICAL IMPLEMENTATION

The ultimate goal is to provide power electronics designers with a tool that will reduce the errors, time and effort spent on extracting and extrapolating parameters from datasheets. In this research, NNALM demonstrates superior accuracy throughout the whole dataset, and it also enables loss maps to account for more factors and generate multiple outputs as both winding and core losses. As a result, the manufacturers can perform all the measurements on representative samples from a batch/design of the component and then generates an NNALM file (e.g., a few kilobytes in size) to distribute to the end-users, which enables rapid, accurate and user-friendly loss estimations. To shift from material-based to component-based datasheets, the NNALM demands large datasets to effectively predict losses of individual components, which is enabled by rapid loss characterization tools/equipment, such as TPT [5], [6], MADMIX [31] and the rig applied in [17]. The power electronics engineers can then incorporate this NNALM file in their analytical models or real-time simulation models as interpolated look-up tables in black boxes to estimate the loss of a standardized magnetics part in their circuits. In this way, power electronics designers will no longer have to spend hours extracting and extrapolating parameters from datasheets prone to error to achieve the ideal inductors and HF transformers design.

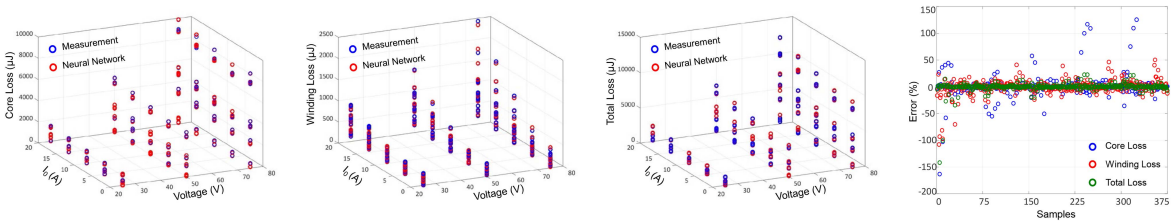

FIGURE 18. The NN predicted and measured losses of the HF transformer for (a) Core losses, (b) Winding losses, (c) Total losses, and (d) the calculated relative error.

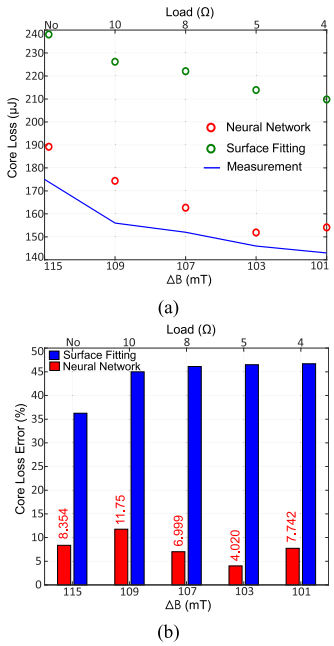

FIGURE 19. (a) The core loss results from measurement, NN, and surface fitting, (b) the calculated error between the measured results and the NN and surface fitting methods.

VI. CONCLUSION

This paper demonstrates using Artificial Neural Networks (ANNs) to aid the generation of user-friendly loss maps as an alternative to traditional datasheets of magnetics. To achieve accurate modelling, an extended range of intercoupled input variables (e.g., DC bias and load conditions) and output variables (e.g., both the core loss and copper loss) can be realized in ANN-aided loss maps. According to the results, the proposed NNALM can achieve consistent and accurate fitting of measured losses under various conditions, which shows less than 10% average error. Comparisons reveal that the conventional loss maps can lose accuracy due to oversimplifications of physically interlinked variables as limited by the allowable dimensions in classic curve/surface fitting. Moreover, thanks to the ease of training, the NNALM can adapt to the increased fitting demand to shift from material-based to component-based datasheets for magnetics, improving accuracy by factoring in the geometry-related, component-specific, large-signal effects (e.g., gap losses). The NNALM file, which is only a few kilobytes in size, can be generated by the manufacturers and distributed to the end users for individual standardized magnetics.

REFERENCES

[1] K. Venkatachalani, C. R. Sullivan, T. Abdallah, and H. Tacca, "Accurate prediction of ferrite core loss with non-sinusoidal waveforms using only Steinmetz parameters," in *Proc. IEEE Workshop Comput. Power Electron.*, 2002, pp. 36–41.

[2] C. R. Sullivan, "High frequency core and winding loss modeling," in *Proc. IEEE Int. Electric Mach. Drives Conf.*, 2013, pp. 1482–1499.

[3] Y. Wang, G. Calderon-Lopez, and A. J. Forsyth, "High-frequency gap losses in nanocrystalline cores," *IEEE Trans. Power Electron.*, vol. 32, no. 6, pp. 4683–4690, Jun. 2017.

[4] J. Muhlethaler, J. Biela, J. W. Kolar, and A. Ecklebe, "Core losses under the DC bias condition based on Steinmetz parameters," *IEEE Trans. Power Electron.*, vol. 27, no. 2, pp. 953–963, Feb. 2012.

[5] J. Wang, K. J. Dagan, X. Yuan, W. Wang, and P. H. Mellor, "A practical approach for core loss estimation of a high-current gapped inductor in PWM converters with a user-friendly loss map," *IEEE Trans. Power Electron.*, vol. 34, no. 6, pp. 5697–5710, Jun. 2019.

[6] J. Wang, X. Yuan, and N. Rasekh, "Triple pulse test (TPT) for characterizing power loss in magnetic components in analogous to double pulse test (DPT) for power electronics devices," in *Proc. 46th Annu. Conf. IEEE Ind. Electron. Soc.*, 2020, pp. 4717–4724.

[7] J. Wang, N. Rasekh, X. Yuan, and K. J. Dagan, "An analytical method for fast calculation of inductor operating space for high-frequency core loss estimation in two-level and three-level PWM converters," *IEEE Trans. Ind. Appl.*, vol. 57, no. 1, pp. 650–663, Jan./Feb. 2021.

[8] T. Shimizu and S. Iyasu, "A practical iron loss calculation for AC filter inductors used in PWM inverters," *IEEE Trans. Ind. Electron.*, vol. 56, no. 7, pp. 2600–2609, Jul. 2009.

[9] H. Matsumori, T. Shimizu, K. Takano, and H. Ishii, "Evaluation of iron loss of AC filter inductor used in three-phase PWM inverters based on an iron loss analyzer," *IEEE Trans. Power Electron.*, vol. 31, no. 4, pp. 3080–3095, Apr. 2016.

[10] H. Matsumori, T. Shimizu, X. Wang, and F. Blaabjerg, "A practical core loss model for filter inductors of power electronic converters," *IEEE J. Emerg. Sel. Topics Power Electron.*, vol. 6, no. 1, pp. 29–39, Mar. 2018.

[11] N. Rasekh, J. Wang, and X. Yuan, "A new method for offline compensation of phase discrepancy in measuring the core loss with rectangular voltage," *IEEE Open J. Ind. Electron. Soc.*, vol. 2, pp. 302–314, 2021.

[12] N. Rasekh, J. Wang, and X. Yuan, "The variation of core loss in high-frequency transformers under different load conditions," in *Proc. IEEE 24th Eur. Conf. Power Electron. Appl.*, 2022, pp. P.1–P.10.

[13] N. Rasekh, J. Wang, and X. Yuan, "A novel in-situ measurement method of high-frequency winding loss in cored inductors with immunity against phase discrepancy error," *IEEE Open J. Ind. Electron. Soc.*, vol. 2, pp. 545–555, 2021.

[14] N. Rasekh, J. Wang, and X. Yuan, "In-situ measurement and investigation of winding loss in high-frequency cored transformers under large-signal condition," *IEEE Open J. Ind. Appl.*, vol. 3, pp. 164–177, 2022.

[15] H. Li, S. R. Lee, M. Luo, C. R. Sullivan, Y. Chen, and M. Chen, "MagNet: A machine learning framework for magnetic core loss modeling," in *Proc. IEEE 21st Workshop Control Model. Power Electron.*, 2020, pp. 1–8.

[16] E. Dogariu, H. Li, D. S. López, S. Wang, M. Luo, and M. Chen, "Transfer learning methods for magnetic core loss modeling," in *Proc. IEEE 22nd Workshop Control Model. Power Electron.*, 2021, pp. 1–6.
[17] H. Li et al., "Magnet: An open-source database for data-driven magnetic core loss modeling," in *Proc. IEEE Appl. Power Electron. Conf. Expo.*, 2022, pp. 588–595.
[18] D. Serrano et al., "Neural network as datasheet: Modeling B-H loops of power magnetics with sequence-to-sequence lstm encoder-decoder architecture," in *Proc. IEEE 23rd Workshop Control Model. Power Electron.*, 2022, pp. 1–8.
[19] J. Y. Alsawalhi and S. D. Sudhoff, "Saturable thermally-representative Steinmetz-based loss models," *IEEE Trans. Magn.*, vol. 49, no. 11, pp. 5438–5445, Nov. 2013.
[20] J. Liu, Y. Mei, S. Lu, X. Li, and G.-Q. Lu, "Continuously variable multi-permeability inductor for improving the efficiency of high-frequency DC-DC converter," *IEEE Trans. Power Electron.*, vol. 35, no. 1, pp. 826–834, Jan. 2020.
[21] W. A. Roshen, "Fringing field formulas and winding loss due to an air gap," *IEEE Trans. Magn.*, vol. 43, no. 8, pp. 3387–3394, Aug. 2007.
[22] J. Schmidhuber, "Deep learning in neural networks: An overview," *Neural Netw.*, vol. 61, pp. 85–117, 2015.
[23] Y. LeCun, Y. Bengio, and G. Hinton, "Deep learning," *Nature*, vol. 521, pp. 436–444, May 2015.
[24] S. Zhao, F. Blaabjerg, and H. Wang, "An overview of artificial intelligence applications for power electronics," *IEEE Trans. Power Electron.*, vol. 36, no. 4, pp. 4633–4658, Apr. 2021.
[25] T. Guillod, P. Papamanolis, and J. W. Kolar, "Artificial neural network (ANN) based fast and accurate inductor modeling and design," *IEEE Open J. Power Electron.*, vol. 1, pp. 284–299, 2020.
[26] E. I. Amoiralis, P. S. Georgilakis, T. D. Kefalas, M. A. Tsili, and A. G. Kladas, "Artificial intelligence combined with hybrid FEM-BE techniques for global transformer optimization," *IEEE Trans. Magn.*, vol. 43, no. 4, pp. 1633–1636, Apr. 2007.
[27] C. Nussbaum, H. Pfutzner, T. Booth, N. Baumgartinger, A. Ilo, and M. Clabian, "Neural networks for the prediction of magnetic transformer core characteristics," *IEEE Trans. Magn.*, vol. 36, no. 1, pp. 313–329, Jan. 2000.
[28] G. K. Miti and A. J. Moses, "Neural network-based software tool for predicting magnetic performance of strip-wound magnetic cores at medium to high frequency," *IEE Proc. Sci. Meas. Technol.*, vol. 151, no. 3, pp. 181–187, May 2004.
[29] Micrometals, "T184-26 datasheet," Accessed: Nov. 2022. [Online]. Available: https://datasheets.micrometals.com/T184-26-DataSheet.pdf
[30] D. Santamargarita, G. Salinas, D. Molinero, E. Bueno, and M. Vasić, "Trade-off between accuracy and computational time for magnetics thermal model based on artificial neural networks (ANN)," *IEEE J. Emerg. Sel. Topics Power Electron.*, early access, Sep. 01, 2022, doi: 10.1109/JESTPE.2022.3203934.
[31] MADMIX Power inductor measurement, Accessed: Oct. 2022. [Online]. Available: http://www.mindcet.com/measurement-systems/madmix

NAVID RASEKH (Graduate Student Member, IEEE) received the B.Sc. degree in electrical engineering from the Kermanshah University of Technology, Kermanshah, Iran, in 2015, and the M.Sc. degree in electrical engineering from the Amirkabir University of Technology, Tehran, Iran, in 2018. He is currently working toward the Ph.D. degree with the Electrical Energy Management Group, University of Bristol, Bristol, U.K. His research interests include designing and controlling high-power/high-frequency converters, modelling and measuring magnetic component losses, wireless power transfer, and finite element analysis.

JUN WANG (Member, IEEE) received the B.S. degree in electrical engineering from Sichuan University, Chengdu, China, the M.Sc. degree in electrical engineering from the University of Nottingham, Nottingham, U.K., in 2014, and the Ph.D. degree in power electronics from the University of Bristol, Bristol, U.K., in 2019. He is currently a Lecturer and Member of the Electrical Energy Management Group, University of Bristol. His research interests include PWM power converters, wide-bandgap semiconductors, multilevel converter topologies, modelling of high-frequency losses, system-level design optimization, and electric vehicles.

XIBO YUAN (Senior Member, IEEE) received the B.S. degree in electrical engineering from the China University of Mining and Technology, Xuzhou, China, and the Ph.D. degree in electrical engineering from Tsinghua University, Beijing, China, in 2005 and 2010, respectively. In 2017, he became a Professor with the University of Bristol, Bristol, U.K. He is currently the Director of the U.K. National Centre for Power Electronics. His research interests include power electronics and motor drives, wind power generation, multilevel converters, application of wide-bandgap devices, electric vehicles, and more electric aircraft technologies. He holds the Royal Academy of Engineering/Safran Chair of advanced aircraft power generation systems. He is a Distinguished Lecturer of IEEE Power Electronics Society. He is also a Fellow of IET. He was the recipient of The Isao Takahashi Power Electronics Award in 2018.